Quaternary International 274 (2012) 25–37

Contents lists available at SciVerse ScienceDirect

Quaternary International

journal homepage: www.elsevier.com/locate/quaint

Climatic change recorded in the sediments of the Chew Bahir basin, southern Ethiopia, during the last 45,000 years

Verena Foerster [a,*], Annett Junginger [c], Oliver Langkamp [a], Tsige Gebru [a], Asfawossen Asrat [d], Mohammed Umer [d,1], Henry F. Lamb [e], Volker Wennrich [b], Janet Rethemeyer [b], Norbert Nowaczyk [f], Martin H. Trauth [c], Frank Schaebitz [a]

[a] Seminar of Geography and Education, University of Cologne, Gronewaldstraße 2, 50931 Köln, Germany
[b] Institute of Geology and Mineralogy, Zülpicher Straße 49a–b, 50674 Köln, Germany
[c] University of Potsdam, Institute of Earth and Environmental Science, Karl-Liebknecht-Straße 24, 14476 Potsdam-Golm, Germany
[d] University of Addis Ababa, Department of Earth Sciences, P.O. Box 1176, Addis Ababa, Ethiopia
[e] Institute of Geography and Earth Sciences, Aberystwyth University, Aberystwyth SY23 3DB, United Kingdom
[f] GFZ German Centre for Geoscience Potsdam, Helmholtz Centre Potsdam, Telegrafenberg C321, 14473 Potsdam, Germany

ARTICLE INFO

Article history:
Available online 30 June 2012

ABSTRACT

East African paleoenvironments are highly variable, marked by extreme fluctuations in moisture availability, which has far-reaching implications for the origin, evolution and dispersal of *Homo sapiens* in and beyond the region. This paper presents results from a pilot core from the Chew Bahir basin in southern Ethiopia that records the climatic history of the past 45 ka, with emphasis on the African Humid Period (AHP, ~15–5 ka calBP). Geochemical, physical and biological indicators show that Chew Bahir responded to climatic fluctuations on millennial to centennial timescales, and to the precessional cycle, since the Last Glacial Maximum. Potassium content of the sediment appears to be a reliable proxy for aridity, showing that Chew Bahir reacted to the insolation-controlled humidity increase of the AHP with a remarkably abrupt onset and a gradual termination, framing a sharply defined arid phase (~12.8–11.6 ka calBP) corresponding to the Younger Dryas chronozone. The Chew Bahir record correlates well with low- and high-latitude paleoclimate records, demonstrating that the site responded to regional and global climate changes.

1. Introduction

Numerous hypotheses claim that there is a link between climate change and human evolution, since climate change provides the necessary environmental pressure for natural selection and population expansion. Various ideas have been put forward about the causes of evolutionary change in the source region of anatomically modern humans (AMH), including climatic variability causing resource stress (Potts, 1998), and adaptation to a gradual shift to a drier environment (Vrba, 1985). Current evidence points to East Africa as the origin of modern humans and thus supports the Out of Africa II or Mitochondrial Eve theory (Stringer, 2003). Much paleontological and paleoanthropological research is focused on the Ethiopian Rift and the Afar, because the oldest known *Homo sapiens* fossils, dated ~200 ka were found in the Lower Omo Valley (McDougall et al., 2005; Carto et al., 2009), and at Herto, in the Afar (White et al., 2003).

Current debate concerns whether the shift towards hyper-arid climate conditions during Heinrich event 9 (H9; 105 ka), resulting in limited resources and water availability, compelled AMH to expand beyond Africa. Environmental changes linked to orbitally-driven dry–wet alternations are thought to have favored evolutionary innovation (Behrensmeyer, 2006; Trauth et al., 2010), and forced the expansion of *H. sapiens* into SW Asia in several intervals at around 100 ka (Ambrose, 1998; Oppenheimer, 2009; Armitage et al., 2011). Whether dry conditions were the driving factor (Carto et al., 2009), plus lowered sea level opening a corridor into SW Asia, or whether it was the onset of wet conditions between ~120 and 110 ka that allowed dispersal into the Arabian coastal desert (Castañeda et al., 2009), is much debated. To understand the

* Corresponding author.
E-mail addresses: v.foerster@uni-koeln.de (V. Foerster), annett.junginger@geo.uni-potsdam.de (A. Junginger), o.langkamp@gmx.de (O. Langkamp), tgebruka@uni-koeln.de (T. Gebru), asfawossena@gmail.com (A. Asrat), hfl@aber.ac.uk (H.F. Lamb), volker.wennrich@uni-koeln.de (V. Wennrich), janet.rethemeyer@uni-koeln.de (J. Rethemeyer), nowa@gfz-potsdam.de (N. Nowaczyk), martin.trauth@geo.uni-potsdam.de (M.H. Trauth), frank.schaebitz@uni-koeln.de (F. Schaebitz).
[1] Deceased.

1040-6182/$ – see front matter © 2012 Elsevier Ltd and INQUA. All rights reserved.
http://dx.doi.org/10.1016/j.quaint.2012.06.028

cause–effect relationships among climate, environment and human evolution in East Africa, it is of key importance to reconstruct the timing and mechanisms of past environmental changes.

The magnitude, timing, spatial expression and causes of wet–dry cycles in East Africa are not well understood. The most recent of these wet episodes, the African Humid Period (AHP, ~15–5 ka), demonstrates the central problem of contradictory data about the timing of these phases (deMenocal et al., 2000; Kröpelin et al., 2008). Using marine records from the northwest African coast, deMenocal et al. (2000) claim an abrupt onset and termination of the AHP, whereas Kröpelin et al. (2008) found a gradual climatic transition at the end of the AHP recorded in lacustrine sediments in the Sahara desert. Each scenario has rather different implications about the pace of human expansion through green corridors of the Sahara. The magnitude of these climate shifts is also important, determining whether they would have allowed relatively moist refugia during dry intervals. The southwestern Ethiopian highlands and the adjacent Chew Bahir and Turkana basins might have formed refugia for human populations during past arid phases (Ambrose, 1998; Hildebrand et al., 2010; Joordens et al., 2011), hosting small but culturally diverse populations of hunter–gatherers, and favoring the development of new food-gathering technologies and cultural skills. If wet phases like the AHP did not occur synchronously in various locations, they could have created refugia for humans and other biota, thus having a major influence on the spatial distribution, size, and movement of human populations. Chew Bahir lies in a possible migration corridor between retreat areas and therefore represents an ideal natural laboratory to study environmental history in the source region of modern humans.

This paper presents results from analysis of a pilot lacustrine sediment core obtained from the Chew Bahir basin in southern Ethiopia (Fig. 1). The core covers paleoenvironmental changes of the past 45 ka years. The data provide valuable insights into the

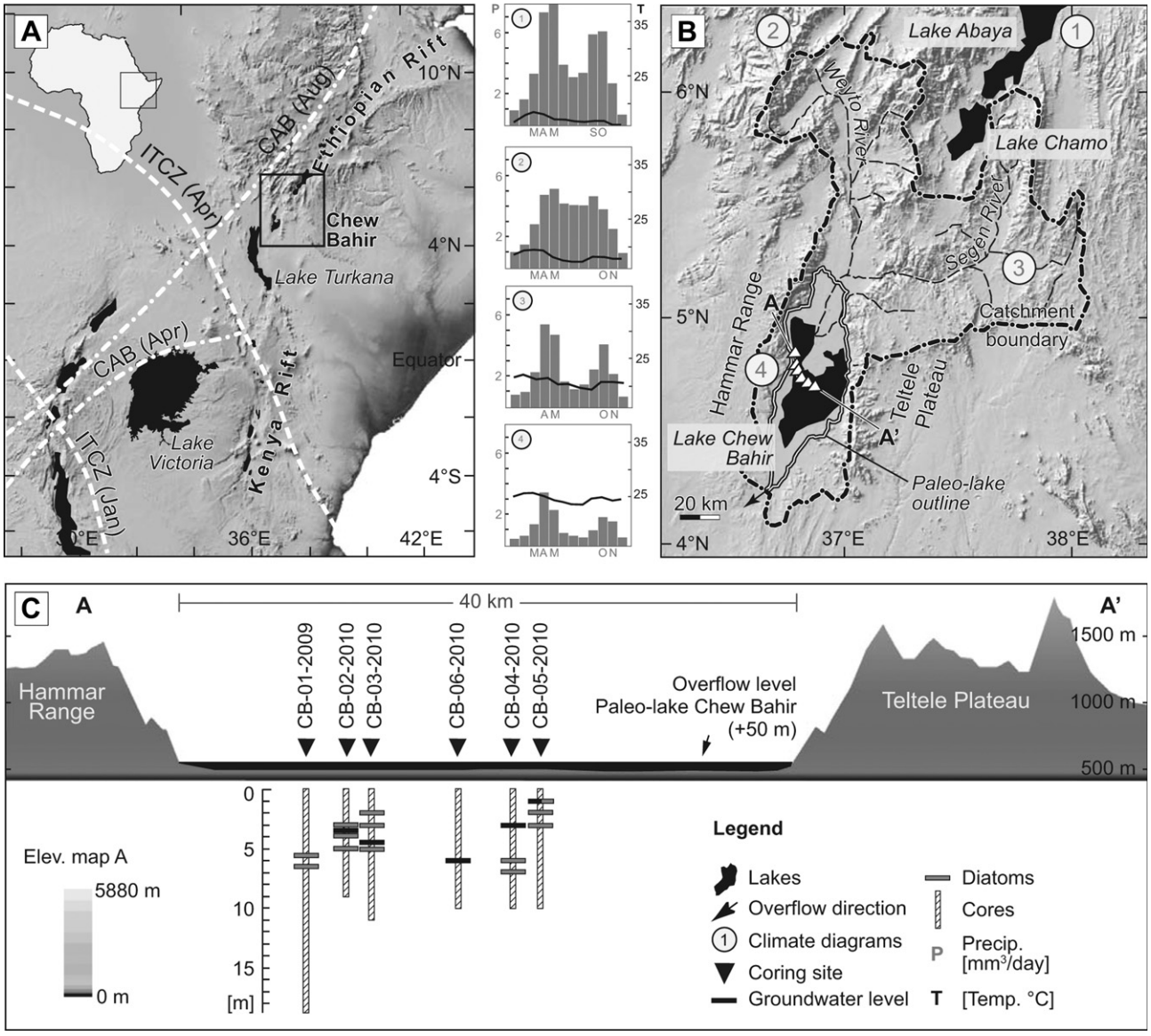

Fig. 1. Setting of the Chew Bahir basin. (A) Chew Bahir basin within the East African Rift System with major climatic influences. Dotted lines indicate the position of the ITCZ (Intertropical Convergence Zone) and CAB (Congo Air Boundary) during different times of the year (after Tierney et al., 2011). (B) Map of the Chew Bahir catchment with major rivers, paleo-lake outline and sites mentioned in the text. Numbers refer to available precipitation and temperature data summarized in climate diagrams between A and B (data: http://iridl.ldeo.columbia.edu/maproom/ – accessed 12.07.2011). A–A′ cross-section along the core transect is provided in (C): Six sediment cores were recovered from a W–E transect through the Chew Bahir basin. Results of the pilot CB-01-2009 core discussed in this study provide paleo-climatic information for the past 45,000 years.

timing, magnitude, synchronicity and internal variability of the most recent, and hence best-studied wet episode, the AHP. This new record of climate change will provide a basis for better understanding the complex interplay between paleoenvironmental changes and the evolution and the dispersal of our ancestors.

2. Setting

2.1. Geological overview

The Chew Bahir basin lies in a 300 km wide rift zone, between the Omo-Turkana basin to the west and the southern sector of the Main Ethiopian Rift (MER) to the east (Fig. 1A). The MER splits into two branches south of the Lake Abaya–Chamo basin, separated by the Amaro horst. The eastern branch forms the southernmost sector of the MER. In the western sector, rift faulting dies out at the southern shore of Lake Chamo close to the Konso uplands, but resumes farther west in the Chew Bahir basin. The Chew Bahir basin extends south to the Kenyan Rift and forms the northernmost part of the broadly rifted zone that was formed when rifting migrated eastward along pre-rift structures of the Anza Rift (Ebinger et al., 2000; Corti, 2009).

The western boundary of Chew Bahir basin, the Hammar range, consists of Precambrian basement with mainly undivided gneisses (units "Pebh" and "Pegh" in Fig. 2). This comprises feldspar–biotite–muscovite and hornblende gneisses dominating the Hammar range geology, migmatitic in part, with minor metasedimentary gneiss (Pegb), quartzo-feldspathic gneiss, amphibolite and granitoid orthogneiss, layered biotite–quartz–feldspar gneiss, locally with muscovite, garnet, sillimanite, minor interlayered amphibolithic quartzose inclusions (Davidson, 1983). In addition, Precambrian layered mafic gneiss (Pegh) and amphibolite or equivalent granulite facies (Pgh) occur in the Hammar range as well as north of the basin.

The higher eastern boundary of the Chew Bahir basin, the escarpment of the Teltele–Konso range, exposes Miocene basalts and trachytic centers (unit "NM" in Fig. 2). Miocene basaltic lava flows with subordinate rhyolite–trachyte and felsic tuff intercalations prevail in the eastern part of the catchment. Oligocene basalt flows with subordinate rhyolites, trachytes, tuffs and ignimbrites (unit "Pv" in Fig. 2) cover the Precambrian basement units in the northeastern, northern and northwestern parts of the catchment (Figs. 1B and 2; Moore and Davidson, 1978; Davidson, 1983).

The tectonically-formed basin provides a sedimentary archive that extends beyond the Quaternary as the basin emerged during older phases of rifting. The total sediment infill of the basin is ~5 km thick, according to airborne gravity and seismic reflection data (Asrat et al., 2009). A detailed spatial and temporal quantification of uplift and denudation along the Hammar and Teltele ranges adjoining the Chew Bahir basin showed that rifting has been continuous since its initiation in the Miocene, while Plio-Pleistocene rifting and uplift was not significant in this part of the East African Rift (Ebinger et al., 2000; Pik et al., 2008). It was further suggested that direct evidence of denudation is inconsistent with the hypothesis that massive Plio-Pleistocene rifting and associated uplift occurred in this part of the East African Rift and could have triggered recent aridification. Other studies (e.g., Ebinger et al., 2000) also suggested similar ages and processes of rifting for this basin. In short, recent tectonic uplift had little influence on the short-term climatic variations.

Today, Chew Bahir is a 30 × 70 km saline mudflat that episodically fills to a shallow lake during the rainy season, with water and sediment input by the perennial Weyto and Segen rivers, which have a ~2000 km^2 catchment (Fig. 1B; 4.1–6.3°N; 36.5–38.1°E;

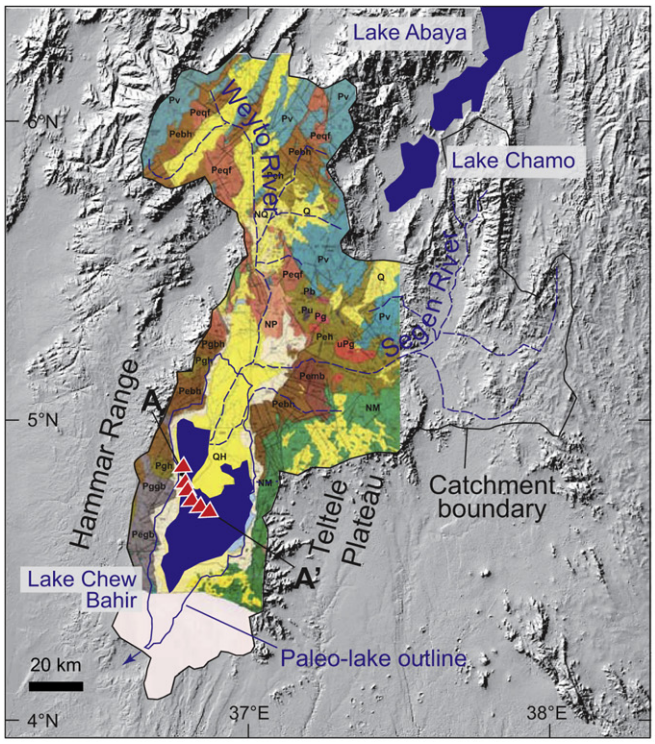

Legend

Q; QH; NQ	Holocene (QH), Plio-Pleistocene (NQ) and Pleistocene-Holocene (Q) undivided fluviatile, alluvial, and lacustrine sediments
QHi	Holocene (QHi)
NP	Pliocene undivided sediments
NM	Miocene basalt, rhyolite, trachyte, phonolithe, ignimbrite
Pv	Oligocene basalt, rhyolite, trachyte, tuff, ignimbrite
uPg	Late precambrian post-tectonic granite, granodiorite, minor syenite
Pggb; Pegb	Precambrian granulite facies (Pggb) or metasedimentary gneiss (Pegb): layered biotite-quartz-feldspar gneiss, locally with muscovite, garnet, sillimanite, minor interlayered amphibolithic quartzose, pyritic, graphitic, and calc-sillicate gneisses, and marble
Peh; Pgh	Precambrian (Pegh) layered mafic gneiss , and amphibolite or equivalent granulite facies (Pgh) including two-pyroxene granulite
Pebh; Pegh	Precambrian undivided gneiss (Pebh): indludes predominantly biotite and hornblende gneiss, migmatitic in part, with minor metasedimentary gneiss, quartzo-feldspathic gneiss, amphibolite and granitoid orthogneiss or equivalent Granulite facies (Pegh) including hyperstene-bearing rocks
Peqf; Pyqf	Precambrian leucocretic biotite-quartz-feldspar gneiss (Peqf) or equivalent granulite facies (Pyqf) including magnetite-quartz-feldspar granulite
Pemb	Precambrian muscovite-biotite granitoid gneiss and migmatite
Pg	Precambrian syn-tectonic granite, granodiorite, minor syenite
Pb; Pu	Precambrian gabbro (Pb) and periodotite, bronzitite, minor dunite, associated layered norite and gabbro, secondary diorite, serpentinite and talc schist (Pu)

Fig. 2. Present available geological information for the catchment of the Chew Bahir basin provided by the Omo River Project (Davidson, 1983).

Davidson, 1983). Their influence is now limited to the northern part of the basin, where the rivers have formed a delta. Secondary, contributions to the sediment influx are alluvial fans draining from the Hammar Range to the west and the Teltele Plateau to the east. Small drainage networks at the border faults, and the strong rainfall seasonality, make sediment and water influx highly episodic, because runoff is mainly from intense rainfall events in the wet seasons, and from occasional orographic rainstorms.

Eolian input, mainly of silt, may be important, especially during dry periods, and can be regarded as a fourth sediment source. Eolian activity may also cause erosion and thus hiatuses in the sedimentary record. Winds transport material from surrounding regions, and redeposit silts within the Chew Bahir basin itself. Minor sources of sediment are volcanic materials, deposited either

as pyroclastic airfall deposits, or as reworked tephra. No volcanic centers are exposed within the Chew Bahir basin. Tephrochronological correlations between the Indian Ocean, the Middle Awash and the Omo-Turkana basin represent explosive volcanic events that affected the entire region. Five dated marker tuffs are of interest, especially the Konso Silver Tuff dated to 154 ± 7 ka, which lies within the timeframe of *H. sapiens* presence in the area (Clark et al., 2003; Brown and Fuller, 2008; Asrat et al., 2009).

2.2. Present-day climate

The climate of East Africa is characterized by strong rainfall seasonality, which results from the annual migration of the Intertropical Convergence Zone (ITCZ) between 10° North and South, following the zenithal position of the sun (Fig. 1A; Nicholson, 1996). Because of this migration, bimodal rains dominate the northeast – the "Belg" rains from March to May, and the longer "Kiremet" rains from June to September. In the highlands northwest of Chew Bahir, rainfall is unimodal with one wet season from March to November (Fig. 1B; Segele and Lamb, 2005; Williams and Funk, 2011). Chew Bahir lies in a transition zone between the influences of tropical equatorial and summer monsoonal climates, and between two major systems that bring precipitation from the Indian and Atlantic Oceans.

The northernmost position of the ITCZ in July–August allows a southwestern humid air stream with recycled eastern Atlantic moisture to reach parts of East Africa via the Congo basin (Fig. 1A; Nicholson, 1996; Camberlin, 1997). This unstable flow from the Atlantic converges with drier air from the Indian Ocean along a northeast–southwest trending convergence zone known as the Congo Air Boundary (CAB). During periods with an intensified Indian Summer Monsoon (ISM), the CAB is thought to bring wet spells even farther east to equatorial East Africa in July and August (Camberlin, 1997; Okoola, 1999; Junginger, 2011). Camberlin (1997) showed that an anomalous deep low over western India enhances the east–west pressure gradient between Africa and India, which results in increased westerly winds from the Congo basin causing the CAB to shift even further eastwards. Thus, the CAB plays a major role in inter-annual moisture variability (Camberlin and Philippon, 2002). Other mechanisms responsible for inter-annual variability are linked to sea surface temperature (SST) anomalies such as the Indian Ocean Dipole (IOD) and El Niño/Southern Oscillation (ENSO) (Diro et al., 2010).

Due to the marked topography of the southern side of the Ethiopian dome, the local climate varies significantly with elevation. A pronounced precipitation, temperature and evaporation gradient lies between the higher areas in the north and the lower basin in the south as well as between the rift valley and the adjacent plateaus. This results in a variety of microclimates, with high rainfall on the cooler highlands draining into the hotter and drier lowlands. The combination of climatology and closed basin morphology allows Chew Bahir to be classified as an amplifier lake, characteristic of the eastern branch of the African Rift (Olaka et al., 2010; Trauth et al., 2010). Those lakes are known to react highly sensitively to even moderate climate changes and thus are potent sites for climate reconstruction.

2.3. Long-term controls on East African climate

Long-term variations of climate are controlled by Milankovitch precessional cycles (19–23 ka), regulating moisture availability in East Africa (Kutzbach and Street-Perrott, 1985); orbitally-forced radiation maxima coincide with increased humidity (Trauth et al., 2003). The most recent of these orbitally controlled dry–wet–dry cycles included the African Humid Period (AHP; ~15–5 ka), which affected large parts of East Africa, as shown by elevated lake-levels at numerous sites (Barker et al., 2004). However, these lacustrine climatic records also show that climate does not respond linearly to precessional insolation change. The transitions are often characterized by an abruptness that can be explained by mechanisms such as climate-biosphere feedbacks functioning as strong amplifiers of basically moderate trends (Renssen et al., 2006; Castañeda et al., 2009). Apart from orbitally-forced variability, centennial-scale variations such as Dansgaard–Oeschger cycles, Heinrich events and the Younger Dryas (YD) have also influenced low-latitude climate, although the sign, magnitude and phasing of their impact are debated (Partridge et al., 2004; Brown et al., 2007; Carto et al., 2009; Chase et al., 2011; Stager et al., 2011). Furthermore, Atlantic and Indian Ocean SST changes, related to the thermohaline circulation, are considered to have a strong influence on African climate (Gasse and Van Campo, 1994; deMenocal et al., 2000; Trauth et al., 2010).

3. Methods

3.1. Core recovery

The pilot sediment core CB-01-2009 was recovered in December 2009 from the now-dry western margin of the Chew Bahir basin (N 04°50′6; E 36°46′8) close to the distal margin of the Weyto-Segen delta, and near an alluvial fan extending eastwards from the Hammar range (Fig. 1B, C). A rotary single tube drill provided by Addis Geosystems Ltd was used for the entire core. The sediment record covers the uppermost 18.86 m of the deposits with a recovery rate of 81%. Coring consisted of 19 drives without overlap. In addition, five short cores (9–11 m length) were drilled with a vibro-corer along an NW-SE transect across the basin (Fig. 1B, C) during a second field campaign in November 2010 and are currently under investigation.

3.2. Chronology

Age control is provided by six AMS radiocarbon ages (Table 1). One organic bulk sample was taken in the field and sent to Beta

Table 1
Radiocarbon data from the Chew Bahir sediment core CB-01-2009.

Laboratory no.	Depth [cm]	^{14}C age [yrs BP]	Calibrated age [yrs calPB]	2-sigma probability	Material	δ^{13}C [‰]	^{14}C conc. [pMC]	Pretreatment
Col 1093.1.1	153	1236 ± 27	1133 ± 60	56.10%	M	−1.4 ± 0.0	85.47	H_2SO_4
Col 1094.1.2	299	3077 ± 27	3301 ± 70	92.80%	M	17 ± 0.0	68.18	H_2SO_4
Beta 271307	735	11790 ± 60	13625 ± 150	95.40%	B	−22.6	N.N.	Acid washes
Col 1095.1.1	976	31085 ± 185	35674 ± 630	95.40%	M	0.8 ± 0.0	2.09	H_2SO_4
Col 1096.1.2[a]	1278	35508 ± 581	40473 ± 1280	95.40%	M	10.1 ± 0.1	1.20	H_2SO_4
Col 1097.1.1	1746	40293 ± 545	44188 ± 920	95.40%	M	0.9 ± 0.0	0.66	H_2SO_4

M – mollusc shells, B – bulk.
[a] The sample was measured only on time in the AMS.

Analytic Inc. in Florida for dating. Five dates were obtained from picked shells and shell fragments of *Melanoides tuberculata*, which were pre-treated and converted to AMS graphite cathodes at Cologne (Rethemeyer et al., in press; Wacker et al., submitted for publication) and measured with the MICADAS AMS at ETH Zürich. The conventional ages were calibrated using the OxCal v4.1.7 calibration software (Bronk Ramsey, 2010; calibration curve: IntCal09; Reimer et al., 2009). To date, no information about a possible reservoir effect on the ages of the carbonate material is available.

3.3. Sedimentological investigations

Core sections were split lengthwise, and the archive halves wrapped in clingfilm to prevent desiccation, and stored in a dark cold storage room. Magnetic susceptibility (MS) was logged to detect variations in grain size, in the flux of magnetic mineral particles from soils and rocks, and volcanic ash layers. Magnetic susceptibility was obtained every 1 mm using a 2nd generation split-core logger (scl-2.3) designed at the Helmholtz Centre Potsdam GFZ. Magnetic susceptibility was measured with a Bartington MS2E spot-reading sensor attached to an MS2 control unit. Element content of the sediment core was determined by X-ray fluorescence (XRF) with an Itrax®core scanner using a Molybdenum (Mo) tube as radiation source. The prepared core halves were scanned at 0.5 cm resolution and a tube voltage of 30 kV, current of 30 mA and scanning time of 20 s.

After the non-destructive measurements, the working half was subsampled at 2 cm intervals. To avoid contamination, 0.5 cm of the core surface was first removed. Half of each sample was freeze-dried and ground for mineral, carbon and nitrogen analysis. Sediment color was defined using a Munsell soil color chart. Grain size and composition was determined by a semi quantitative finger-test, differentiating crudely between finer and coarser material in five increments (clay, silty clay, silt, sandy silt, sandy gravel; simplified in Fig. 3). Also the mineral content was determined semi quantitatively, by X-ray diffraction (XRD) analysis of finely ground bulk samples, without further treatment or adding a standard indicator, using a Siemens D5000 diffractometer and EVA for phase identification.

The biogeochemical indicators Total Nitrogen (TN) and Total Carbon (TC) have been analyzed along the core in a ~32 cm resolution. TC has been differentiated into Total Inorganic Carbon (TIC) and Total Organic Carbon (TOC) and TOC/TN ratios have been calculated to distinguish between terrestrial and aquatic carbon sources. However, with very low TN values (ranging from 0.01 to 0.04 wt%) as well as a low TOC content (variations between 0.1 and 0.3 wt%), neither the values nor the variability of the ratios are significant enough and are therefore excluded from further discussion (Meyers, 2003).

Smear slide analyses were conducted on the non-ground half of subsamples along the entire core at ~30 cm intervals and in selected sections at higher resolution to gain initial insight about sediment composition and possible biological indicators, such as pollen, diatoms, ostracods and charcoal. For diatom identification,

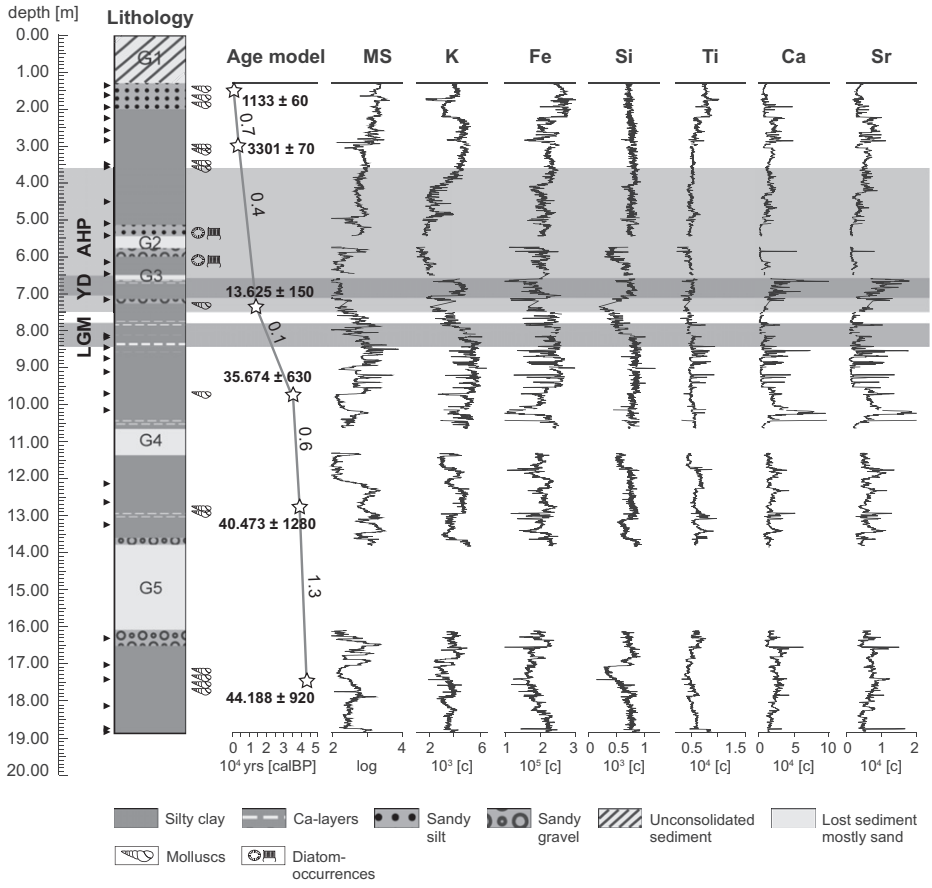

Fig. 3. Lithology, age-depth model and results of geochemical and physical investigations of the pilot core CB-01-2009. Numbers along the age model present sedimentation rates in mm/year. Stars – ^{14}C ages; triangles – XRD samples; MS – Magnetic Susceptibility; LGM – Last Glacial Maximum; YD – Younger Dryas; AHP – African Human Period; G1–G5 – gaps in the record due to lost/unconsolidated sediment.

selected samples were treated with KOH and examined under an electron microscope. For semi-quantitative analyses following the principles of Gasse (1986), light microscopy was used, complemented with a polarizer.

4. Results

4.1. Core description

The pilot core CB-01-2009 was drilled to 18.86 m depth without replicate coring so that due to a 19% core loss the recovered material comprises 15.36 m in total. Five gaps interrupt the profile (Fig. 3; G1–G5), because of unconsolidated sediments (G1) and material that was not completely recovered (mostly sand) or lost due to technical limits (G2–G5). The topmost section (G1; 0–130 cm) of the core has been subjected to soil formation expressed in unconsolidated sediment. The hiatuses as well as the unconsolidated section were unavailable for continuous geophysical and chemical measurements and therefore did not provide data. The lithology of the rest of the core comprises lacustrine unlaminated silty clays, which are intercalated with sandy layers and coarse detrital fragments. In the lowermost section, prominent carbonate layers mark parts of the lacustrine sequence. Up to six horizons with abundant gastropods *M. tuberculata* occur in different matrixes from silty clay to sandy gravel.

4.2. Age model and sedimentation rates

The radiocarbon ages of biogenic carbonates and one bulk sediment sample (Table 1) are consistent with their depths, showing no reversals. Both linear model and cubic spline models were calculated from the radiocarbon ages, but these show only minor statistical deviations for the intervals of higher sedimentation rate between 150 and 300 cm and between 1280 and 1750 cm.

The estimated sedimentation rate for the interval between 45 and 40 ka is relatively high with a time-averaged value of 1.3 mm/a. After 40 ka, sedimentation rates decreased first to 0.6 mm/a (between ~40 and 35 ka) and then to only 0.1 mm/a between 35 and 13 ka. Towards the present, the sedimentation rate increases again in two steps, first slowly with values of 0.4 mm/a between 13 and 3 ka and 0.7 mm/a between 3 and 1 ka, reaching 1.3 mm/a during the last 1000 years (Fig. 3). The mean sedimentation rate for the last 45 ka is ~0.7 mm/a. Stratigraphic changes in core sediment composition and grain size almost certainly reflect additional, short-term variations in sedimentation rate that are not apparent from interpolation between dated levels.

4.3. Sedimentological results

As the uppermost section has been subjected to soil formation, all scanning and logging results start at 130 cm depth (Fig. 3). The sediment color changes from green–gray shades at the base to brown, green–brown, gray–brown and light brown Towards the top. The MS log shows generally higher values within coarser layers such as sandy silts and gravels. Some higher values in the silty clays may be attributed to non-detectable grain size variations due to the semi-quantitative method used. Higher MS fluctuations are observed between the base of the core and ~8 m depth; low values follow with lowest variability to ~6 m depth, followed by gradually increasing values, but still with very low internal variability.

Initial XRD results show that mineral assemblages vary along the core. A mixture of potassium feldspars and potassium–sodium feldspars are main constituents of the spectrum, in particular orthoclase and some sanidine, as well as plagioclase (albite and anorthite). Other mineral phases are illite, analcime, epidote, magnesiohornblende and calcite. From the smectite family, montmorillonite is present in the deposits. Quartz is also an important component of the mineral assemblage (Table 2).

4.4. Geochemistry

The Itrax core scanner provided the element contents for 16 elements, but only 6 of these show a clear paleoenvironmental signal (Fig. 3). All other elements record either a mixed signal with multiple partly anti-correlated or phase shifted signals, or their record does not differ significantly from random noise. Potassium (K) shows marked variation with noticeably abrupt transitions. Its variance changes throughout the core, in a pattern similar to that of MS, with higher short-time amplitudes in the middle and Towards the base of the core, far exceeding the amplitudes in the upper 800 cm. Mean values by contrast, show larger variations in the upper half of the core. The K content is generally higher at the middle of the core but shows from 8 m upwards a rather abrupt change to lower values, gradually returning to an elevated value level at around 4 m, while framing a pronounced short-term fluctuation between 6.50 m and 7.10 m. Iron (Fe) is high throughout the core with some marked variations between 10 and 8 m, and less extreme variations between 14 and 12 m. Abrupt transitions Towards more stable conditions with less variability are apparent in the rest of the core. The Fe distribution along the record largely correlates with the K values, except the long-term mean value decrease described for the K curve between 8 and 4 m, where the Fe concentration on the contrary remains high. Silica (Si) largely follows the K curve but exhibits a generally lower variability and with gradual rather than abrupt transitions. The titanium (Ti) curve varies with a low magnitude and has generally lower amplitude short-term variations than the other elements. Calcium (Ca) values follow the macroscopically observed calcite layers and layers with greater snail abundances. Ca content varies around a constant mean, but short-term variations are present throughout the core. Highest variability occurs between 10.5 and 8.5 m, 7.5 and 6.5 m and 3 and 2 m. The strontium (Sr) curve parallels the Ca curve, but with generally lower values. Interestingly, most Ca and Sr peaks show distinct anti-correlations with K and Fe, particularly at 10.4 m, 10.2 m or at 8.5 m and around 7.20 m, 2.2 m and 2.85 m.

4.5. Biological indicators

Smear slide analyses revealed the occurrence of ostracods, charred plant remains and diatoms that are not present throughout the whole core but occur in discrete layers. The sediments do not contain detectable numbers of pollen or spores. Smear slide analyses show a gradual increase in diatom abundance Towards a diatom-rich layer between ~6.20 and ~5.45 m dominated by *Aulacoseira* and *Cyclotella*, but the low absolute numbers and poor species diversity do not allow quantitative estimation of past ecologic conditions in the lake. No indicators for saline conditions were found in the core suggesting that the diatoms only occurred during freshwater episodes. Fragments and complete shells of the gastropod *M. tuberculata* occur in six layers ranging from a few cm to more than 0.5 m thickness Towards the base of the core. The lowermost and largest mollusc layer, from ~17.90 to 12.70 m, is followed by abundant well-preserved shells at 13.10–12.80 m and 9.80–9.75 m. At ~3.90–3.00 m and 2.00–1.52 m several single shells in a clayey matrix and dense fragmented mollusc layers have been identified.

Table 2
Results of XRD analyses.

Family			Potassium Feldspar	Potassium-Sodium Feldspar	Feldspar (Plagioclase)	Feldspar (Plagioclase)	Illite (Clay mineral)	Smectite (Clay mineral)	Carbonate	Zeolite	Sorosilicate	Amphibole
Mineral		Quartz	Orthoclase	Sanidine	Albite	Anorthite	Illite	Montmorillonite	Calcite	Analcime	Epidote	Magnesiohornblende
Chemical formula		SiO_2	$KAlSi_3O_8$	$(K,Na)(Si,Al)_4O_8$	$NaAlSi_3O_8$	$CaAl_2Si_2O_8$	$K_{0.65}Al_{2.0}[][Al_{0.65}Si_{3.35}O_{10}](OH)_2$	$(Na,Ca)_{0.33}(Al,Mg)_2Si_4O_{10}(OH)_2{\cdot}nH_2O$	$CaCO_3$	$NaAlSi_2O_6{\cdot}H_2O$	$Ca_2\{FeAl)Al_2[O\|OH\|SiO_4\|Si_2O_7]$	$Ca_2(Mg, Fe, Al)_5$ (Al, Si) $_8O_{22}(OH)_2$
Sample label	**Depth [cm]**	**Abundance code:** ++ abundant +- major occurrences -+ minor occurrences -- no occurrences										
CB-01-2009-3b-132	132	+ -	+ -	- +	+ +	- -	- -	+ -	+ -	- +	+ -	- -
CB-01-2009-3b-164	163	++	+ -	- +	- -	+ +	+ +	+ +	- -	+ -	- -	- -
CB-01-2009-4a-190	195	++	- -	- -	- -	+ +	- -	+ -	+ -	+ -	- -	- -
CB-01-2009-4a-222	225	++	- -	- -	+ -	+ -	- -	+ -	- +	- +	- +	+ +
CB-01-2009-4a-254	259	++	- -	- -	+ -	+ +	+ +	- +	- +	- +	- -	+ +
CB-01-2009-4c-284	287	+ -	- -	- -	- +	+ +	- +	- +	- +	- +	- -	- +
CB-01-2009-5a-312	318	- +	- -	- -	+ -	- +	+ -	- +	- +	+ -	- +	- +
CB-01-2009-5a-344	349	- +	- -	- -	- +	- +	+ +	- +	+ +	- +	+ -	- +
CB-01-2009-6a-468	451	- +	- -	- -	- +	+ +	+ +	+ +	- +	+ -	- -	- +
CB-01-2009-6b-532	514	- -	- +	- -	+ +	- -	- +	+ +	+ +	- -	- -	- -
CB-01-2009-7a-562	544	- +	- -	- -	+ +	+ +	+ -	+ -	- -	- +	- -	- -
CB-01-2009-7b-656	616	+ -	- -	- -	+ +	+ +	- +	- +	+ +	- +	- -	- -
CB-01-2009-8a-698	648	+ +	- -	- -	- +	+ -	- +	- +	+ +	- +	- +	- +
CB-01-2009-8c-772	719	- +	- -	- -	- +	- +	+ -	- +	+ +	+ +	- +	+ -
CB-01-2009-9-868	813	- -	- -	- -	- +	+ +	- +	- -	++	++	+ -	+ +
CB-01-2009-9-874	818	- -	- -	- -	- +	+ -	+ +	- -	+ +	+ +	+ +	+ -
CB-01-2009-10-910	844	- -	+ -	- +	- -	- -	+ +	+ -	+ +	+ +	+ -	- +
CB-01-2009-10-942	876	- -	+ +	+ -	- -	- -	+ +	+ -	+ +	+ +	+ -	- -
CB-01-2009-10-973	907	- -	- +	- +	- -	- -	++	- -	+ -	++	- +	- -
CB-01-2009-11a-1064	970	- -	- +	- -	- -	- -	+ +	- +	+ +	+ +	- +	- +
CB-01-2009-13a-1268	1148	- -	- +	- -	- -	- -	+ -	- -	+ +	+ +	+ +	- -
CB-01-2009-13a-1332	1212	- +	- +	- +	- -	- -	+ +	- +	+ +	+ +	- +	+ -
CB-01-2009-14a-1386	1263	- -	- +	- -	- -	+ +	+ +	+ -	+ +	+ +	- -	- +
CB-01-2009-15a-1476	1326	- -	- -	- -	+ +	- -	+ -	+ +	- +	+ +	- -	- +
CB-01-2009-15b-1572	1416	- -	- -	- -	- -	- +	- +	+ -	+ -	+ +	- -	+ -
CB-01-2009-17c-1922	1635	- -	- -	- -	- -	+ +	- +	- +	- -	+ -	- -	- +
CB-01-2009-18a-1996	1705	- +	- -	- -	- -	+ -	+ +	+ +	+ +	+ -	- +	- +
CB-01-2009-18b-2034	1741	- +	- -	- -	+ +	+ +	+ +	+ -	+ +	- +	- -	- +
CB-01-2009-19a-2128	1815	- +	- -	- -	- +	+ -	+ -	- +	+ +	+ +	- +	- +
CB-01-2009-19b-2194	1879	- +	- -	- -	- -	- -	+ +	+ -	- +	+ +	+ -	- -
CB-01-2009-19b-2204	1886	- +	- -	- -	+ +	+ -	+ +	+ +	+ +	+ +	+ -	- +
Occurrence and result relevant properties		Gneiss and granitic intrusions; Si as main component.	Major constituent of biotite-quartz - feldspar gneisses forming the Hammar range; **Source of K and Si.**	Common in rhyolites and trachytes; mainly Teltele range.	Na-rich end-member of plagioclase; common alteration product of granitic gneisses.	Ca-rich end-member of plagioclase; commonly available in granitic gneisses.	Weathering product of micas and feldspars; micas such as biotite and muscovites are common in the granites and granitic gneisses of the Hammar range. **Source of K.**	Weathered product of biotite micas.	Evaporite; calcite precipitate.	Primary mineral in analcime basalt and alkaline igneous rocks; zeolites can be of sedimentary origin.	Usually alteration of feldspar, micas; pyroxene, amphibole, garnets in gneisses during low-grade retrograde metamorphism.	Common constituent of mafic gneiss.

5. Discussion

5.1. Core chronology

The age model may be rather limited with six radiocarbon dates, but the sedimentation rates were very linear with two change points and no reversals; therefore given ages might lack high precision, but are reliable. Some very striking well-studied climate events – in particular the Younger Dryas (YD) – occur exactly where they are expected to be (Figs. 4 and 5). Furthermore, this study is not attempting to determine higher frequency climate variations that would require a high-resolution age model. So, according to the age model for the core, CB-01 records climate history spanning from ~44 ka to 1.0 ka, including the Last Glacial Maximum (18–23 ka), the African Humid Period (5–15 ka) and ending with the onset of the Medieval Warm Period (700–1000 BP/950–1250 AD).

Some of the metasedimentary gneisses contain minor intercalated marble units (Davidson, 1983, Fig. 2), and the latter could be possible source of ^{14}C-depleted runoff. The area has no young volcanoes and few hot springs, representing other possible sources for ^{14}C depleted water. The interpretation (below) suggests that the maximum paleo-lake depth was less than 50 m during highstands over the past 45 ka, enabling constant water circulation and thus preventing enrichment with old ^{14}C in the deeper parts. Consequently, these factors may have reduced the chances of old ^{14}C-depleted C entering the basin. Further investigations, such as parallel dating of charcoal and biogenic carbonate will shed light on the reliability of the radiocarbon chronology.

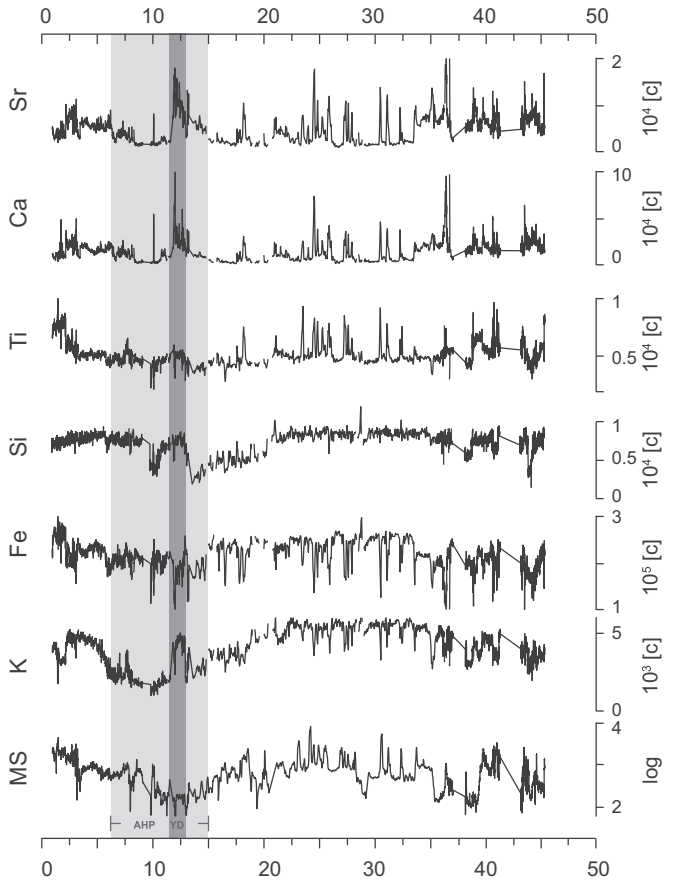

Fig. 4. Results of XRF measurements against time. MS – Magnetic Susceptibility; K – Potassium; Fe – Iron; Si – Silicon; Ti – Titanium; Ca – Calcium; Sr – Strontium; YD – Younger Dryas; AHP – African Human Period.

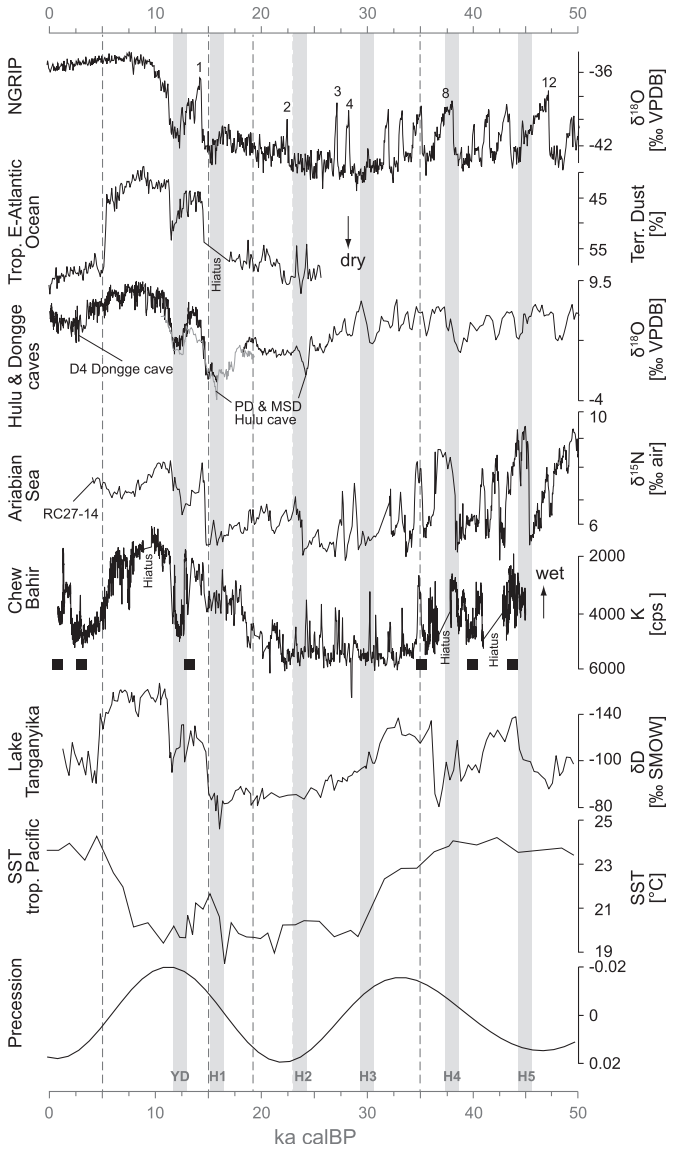

Fig. 5. Comparison of the Chew Bahir potassium (K) record with other paleo-climate records. Records plotted from top to bottom are as follows: δ^{18}O data from NGRIP (North Greenland Ice Core Project members, 2004) with numbers referring to Dansgaard–Oeschger events; terrestrial dust input to the tropical east Atlantic (deMenocal et al., 2000; note reverse scale); δ^{18}O data from Hulu (Wang et al., 2001) and Dongge caves (Dykoski et al., 2005; note reverse scale); δ^{15}N data as proxy for denitrification and productivity in the Arabian Sea in the Gulf of Oman 18°N (Altabet et al., 2002); Chew Bahir potassium (K) record (note reverse scale); Lake Tanganyika δD leaf wax as proxy for precipitation variability (Tierney et al., 2008; note reverse scale); SST (sea surface temperature) record from the eastern Pacific (Martínez et al., 2003) and insolation variations (Berger and Loutre, 1991). Dashed lines indicate time slices discussed in the text. Gray bars refer to Younger Dryas (YD) and Heinrich events H1–H5. The black squares show ^{14}C dates along the Chew Bahir record.

The inferred dry–wet–dry cycles are also expressed in the distinct changes of the sedimentation rate. Especially with the onset of the last humid period 15 ka ago, the sedimentation rate increased significantly by a factor of six to seven between the two dated levels of 35 and 13 ka calBP. Correspondingly, higher sedimentation rates occurred from 45 ka to 35 ka, though interrupted by a large hiatus, which prevents distinguishing whether there was one single continuous humid period or more. Thus, wetter conditions coincide with increased deposition, which is explained by

enhanced fluvial input and connected to a more continuous deposition of generally finer material.

The position of the coring site within this flat basin does not make fluvial erosion and redistribution during lake conditions very likely. However, postulated dry phases indicated by coarser input during strong rain events via the alluvial fan may have also let to a certain amount of fluvial erosion at the coring site, which could not be specified further. If at all, the fluvial erosion is incorporated in the hiatuses G2–G5.

5.2. Evaluation of proxies

The lacustrine sediments of core CB-01-2009 reflect a highly variable environment during the Late Quaternary. The geochemical results concur with physical and biological indicators. The most conspicuous paleoenvironmental indicator is potassium, interpreted as a proxy for aridity in the Chew Bahir catchment. Under generally arid conditions with sparse vegetation cover, the gneisses (e.g., the potassium-rich orthoclase feldspar–biotite–muscovite-gneisses) as well as two-mica granites with conspicuous orthoclase phases constituting the Hammar range are eroded more easily, and then washed into the basin via alluvial fans. These events are expressed by sharp increases of K in the record, reflecting the onset of dry conditions on millennial or even centennial timescales. Increased sediment supply from the alluvial fans of Hammar range during dry conditions into a shallow or even dried out lake also is reflected by coarser material (like sandy silt and sandy gravel; Fig. 3), which is washed in during strong rain events. The K in the record can be attributed exclusively to terrigenous and allochthonous input; and once deposited, no further processes change or enrich the amount of K.

The XRD results show the occurrence of the potassium-rich mineral illite $[(K,H_3O)(Al,Mg,Fe)_2(Si,Al)_4O_{10}[(OH)_2,(H_2O)]$, throughout the stratigraphy, and other potassium-rich minerals, orthoclase (potassium feldspar; $KAlSi_3O_8$), and sanidine $[(K,Na)(Si,Al)_4O_8]$, which occur in the top 30 cm and at 8.44–12.63 depth. Illites are commonly associated with alteration products of micas (biotites and muscovites), and in this case, illites could be alteration products of the feldspathic and micaceous gneisses and granites, which are the dominant rock units forming the Hammar range. The illite content largely correlates with phases of high K values (Table 2). Quartz, which generally is less sensitive to alteration than feldspars and micas, appears especially in the upper levels of the core, almost unaltered. This also suggests a scenario with increased alluvial fan or eolian activity.

Alluvial fans usually become active during occasional short but intense rainfall events instead of evenly distributed rainfall. Moreover, the deposits that are washed in by the Weyto and Segen River from the north of the catchment are rather unlikely to reach the elevated marginal position of CB-01 in a dried out playa scenario or when water level of paleolake Chew Bahir was very shallow.

During wet phases, however, with a higher lake water levels and denser vegetation cover in the catchment area, evenly distributed rains result in the more-or-less continuous discharge of all rivers, transporting more diverse and generally finer material. This also includes Fe- and Ti-rich material input from the basalts constituting the eastern and northeastern ridges surrounding the basin. This input firstly dilutes the already decreased potassium input via the alluvial fan from the Hammar range and secondly mixes in an array of sediments from the entire catchment. Thus, the K record potentially provides a clear aridity signal, as the provenance and transport mechanisms of the element are rather constrained. In support of this dry/wet interpretation, magnetic susceptibility largely parallels the potassium record, despite very coarse layers, where MS is reduced, such as around 7 m. Here, K shows an abrupt return to high values, whereas MS remains low. Richardson and Richardson (1972) employed feldspars and associated elements as indicators for more arid phases and reduced lake levels in the Naivasha basin in central Kenya, arguing that these minerals have been transported to the deposition area by small streams that in turn were associated with larger grain sizes.

The Si distribution along the record largely parallels the potassium record from the base up to ~5.5 m depth, which corresponds to the mid-AHP. This can be explained by a similar provenance as K, because mostly Si – as a quartz (SiO_2) phase – forms a major component of all the quartzo-feldspathic gneisses and the associated micaceous granites of the Hammar range, and during dry intervals Si is subjected to the same transport mechanism. However, during long wetter periods such as the AHP, the lake system stabilizes and biogenic production (e.g., silica rich diatom frustules, see also Fig. 3) increases the amount of Si in the sediment autochthonously. As the XRF results for Si do not differentiate between terrigenous and biogenic Si, the comparison to Ti was used to distinguish between both processes, as the Ti input is exclusively terrigenous. However, Si can be found in most other minerals, as is also clear from Table 2.

Iron (Fe) is another allochthonous component that shows a very similar pattern to Si and especially to K in the lowermost parts of the profile up to 7.8 m depth. As iron is highly redox sensitive, post-sedimentary processes have overprinted the iron signal in the sediment, so iron values differ considerably from potassium, especially during the AHP.

Comparing Fe, K and Si results, it becomes apparent that these elements seem to react very similarly, except during the long wet phases where these three elements show major divergences in trend (Figs. 3 and 4). This has to be attributed to the far more diverse processes (e.g., biogenic production of silica and post-sedimentary reduction of iron) and a more versatile provenance of Fe and Si than K. Whereas K originates mainly from the Hammar range, Fe (found in illite and magnesiohornblende) and Si (mainly from quartz but also common in most felsic minerals) may additionally come from other sources. Iron can be attributed to major Fe-containing mineral phases such as augite, olivine, and hornblende, and to accessory phases such as titanomagnetite from the northeastern and eastern ridges of the catchment (Fig. 2).

Ca and Sr are strongly correlated, indicating a common source and/or transport mechanism. Both elements are present in feldspathic gneisses, granulites and basalts of the catchment area, and are thought to have entered the lake in solution. The cycle of Sr is primarily driven by co-precipitation with authigenic calcite, due to similar ionic radiuses of Ca and Sr, during algal photosynthetic or evaporative precipitation (Stabel, 1987). Additionally, isolated carbonate layers (Fig. 3) throughout the lower part of the core indicate phases of high evaporation that coincide with increased XRF Ca counts (Fig. 4). Therefore, peaks in the Ca record appear at pronounced dry spells, hinting at evaporation. Moreover, enhanced bio-productivity as a second masking process overprints the Ca signal. The onset of heavy rainfalls after drought, bringing nutrients into the lake basin resulted in the increase of the bio-productivity of an existing lake. During these scenarios, Ca and Sr values are high, while K shows a clear anti correlation. This most likely reflects irregular short-term humid events during a period of generally reduced humidity, but still providing enough moisture to sustain at least a shallow lake.

The gastropod *M. tuberculata* occurs in a wide range of fresh and brackish water habitats throughout Africa (Pointier et al., 1992; Leng et al., 1999). Its littoral habitat is mostly associated with aquatic and subaquatic plants in up to 2 m water depth, providing the snails with protection from wave action, as well as food and egg

laying sites (Leng et al., 1999). Some authors report that *M. tuberculata* may live within fine-grained sediment at greater water depths (10–15 m) where they can form high population densities (Pointier et al., 1992). Occurrences of these snail shells in combination with the other proxies indicate water level lowering. These molluscs always appear at the postulated transition zones, indicated by the geochemical proxies for lower water levels and larger grain sizes. Therefore, it seems that these snail shells represent lake levels not deeper than 10 m.

5.3. Paleoclimatic implications for the past 45 ka

The high-resolution K record for the past 45 ka correlates (Fig. 5) with the δD leaf wax record from Lake Tanganyika (Tierney et al., 2008), marine dust records from the Atlantic coast of West Africa (deMenocal et al., 2000) and the Arabian Sea (Altabet et al., 2002), the stable isotope records from Hulu/Dongge Cave in southeast Asia (Wang et al., 2001) and with Greenland ice cores (NGRIP; North Greenland Ice Core Project members, 2004).

Assuming that high values of K reflect aridity, the interval 45–35 ka is characterized by intermediate moisture conditions interrupted by drier periods every ~1000 years. Comparable conditions were also observed in records from Lake Abhé in north Ethiopia (Gasse and Street, 1978) and Lake Tanganyika (Tierney et al., 2008). The two hiatuses in the Chew Bahir record are mostly due to lost sandy material, possibly indicating arid episodes with coarse material transported via the alluvial fan. The arid episode around 37 ka could possibly coincide with the H4 event, which is reported to have caused widespread aridity in East Africa and Asia (Wang et al., 2001; Tierney et al., 2008). The long-term transition to greater humidity from around 35 ka on follows declines in the sea surface temperatures (SST) of the tropical East Pacific leading to generally drier tropical climate during the Last Glacial Maximum (LGM, 18–23 ka; Gasse, 2000; Martínez et al., 2003). A strong temporal relationship between SST cooling of 2–4 °C in the eastern equatorial Pacific and ice sheet growth has been reported leading into a more La Niña like SST field (Clark et al., 2009). According to a model of the response of the NINO3 index, this cooling may have been caused by changes in the low-latitude precession-related insolation (Clement et al., 1999).

Between 35 and 23 ka, even more pronounced aridity dominated the climate in tropical East Africa with short-term shifts Towards humidity indicated by distinct single negative peaks in the K record. In contrast to the time prior to 35 ka, the short-term fluctuations within the overall changes follow a generally decreasing trend. However, the amplitudes of these short-term fluctuations during the LGM far exceed all short-term fluctuations of the past 20 ka. The pattern of these strong short-term variations resembles Dansgaard–Oeschger cycles, and the dry episodes could possibly be interpreted as Heinrich events by tentative correlation with the NGRIP ice core. An African–Asian influence is suggested by correlations with records from Lake Tanganyika, the Arabian Sea and the Hulu/Dongge records (Fig. 5). However, the age model with merely six ages and increasing error bars down-core is not sufficiently precise to correlate dry–wet–dry excursions Towards the core base with Dansgaard–Oeschger cycles.

From 23 ka to 5 ka, K values seem to follow the precession-forced increase in insolation. The time interval between 23 and 19 ka corresponds to the high-latitude LGM, which coincided with pronounced aridity in many parts of tropical Africa and elsewhere in the tropics (Gasse et al., 2008), well reflected by the K record of the Chew Bahir basin. The cooling of the equatorial Atlantic during the LGM reduced moisture transport to the Congo basin via the usually humid Congo air stream, producing higher aridity in the central parts of Africa. Since Chew Bahir lies at the foot of the Ethiopian plateau, it is occasionally influenced by the humid Congo air masses at the present day. Hence, it is possible that what is seen in the K record is the result of a combination of both mechanisms: the insolation forced moisture shifts and the migration of the CAB.

Increased insolation, on the contrary, results in greater humidity at Chew Bahir after 19 ka. However, despite gradual insolation change, the return to more humid conditions occurs in abrupt steps of increasing amplitude at 19–15 ka, 14.5–12.8 ka, and 11.5 ka. Such a stepwise increase in precipitation is also described in various paleoclimatic records from Africa north of 8–9°S (Gasse et al., 2008). The AHP (15–5 ka) is the result of the precessional increase in Northern Hemisphere insolation during low eccentricity (deMenocal et al., 2000; Barker et al., 2004; Garcin et al., 2009). The humid Congo air stream may have again become more influential with the onset of the AHP 15 ka ago as suggested by a recent study from the Suguta Valley, just south of the Chew Bahir basin (Junginger, 2011). Extreme humidity in northern Ethiopia is thought to be the result of an eastward shift of the CAB due to a deepening of the atmospheric low over India causing an enhanced pressure gradient between India and Asia (Hailemichael et al., 2002). The combination of rising SSTs providing more moisture and additional continuous moisture availability during the present dry season via the CAB may have caused the pronounced humid episode in the Chew Bahir basin.

According to the age model, a rapid shift Towards extreme arid conditions is indicated by increased K values around 12.8 ka, before returning to wet conditions at 11.6 ka, as reflected by a steep decrease of K. This dramatic arid event within the orbitally-controlled humid interval correlates with the high-latitude Younger Dryas event (YD, 12.8–11.6 ka) that coincides with arid conditions everywhere in Africa north of 10°S (Barker et al., 2004; Gasse et al., 2008; Tierney et al., 2011). The K data indicate a short-term return to humid conditions around 11.8 ka ago in Chew Bahir, but the final return to full humid conditions started abruptly around 11.6 ka, within about 200 years. This rapid termination of the YD is also documented in other East African paleoclimatic records, such as the onset of ice accumulation on Mt. Kilimanjaro with the tentative age of 11.65 ka (Thompson et al., 2002) and rapid regressions of lakes Nakuru (Richardson and Dussinger, 1986), Suguta (Junginger, 2011), Abiyata (Chalié and Gasse, 2002) and Ziway-Shala (Gillespie et al., 1983) (Fig. 5). It is also suggested in various studies from West Africa (e.g., deMenocal et al., 2000; Shanahan et al., 2006) and Asia (e.g., Wang et al., 2001; Yuan et al., 2004).

Having returned to maximum humid conditions after the YD, multiple fluctuations in the K, Ca and Sr records indicate a series of brief drier intervals around 10.8–10.5 ka, 9.8–9.1 ka (hiatus due to unconsolidated sands), followed by a gradual decrease of moisture between 8.0 and 7.5 ka and an abrupt major drought event around 7 ka (Fig. 6). Most of these events have been described as abrupt phases of maximum aridity during the AHP throughout East Africa from various archives including dust events in the Kilimanjaro ice record (Thompson et al., 2002), lake-level variations, and changes in diatom assemblages (Telford and Lamb, 1999; Gasse, 2000; Guo et al., 2000; Chalié and Gasse, 2002).

The termination of the AHP in the Chew Bahir basin according to the K record started around 6 ka ago and continued for 1000 years until full arid conditions were reached at 5 ka. This gradual climate change contrasts with the abrupt termination of the AHP recorded in marine archives (deMenocal et al., 2000; Renssen et al., 2006; Garcin et al., 2009). These records and climate modelling results indicate a more abrupt decline of the AHP between 5 and 4.5 ka

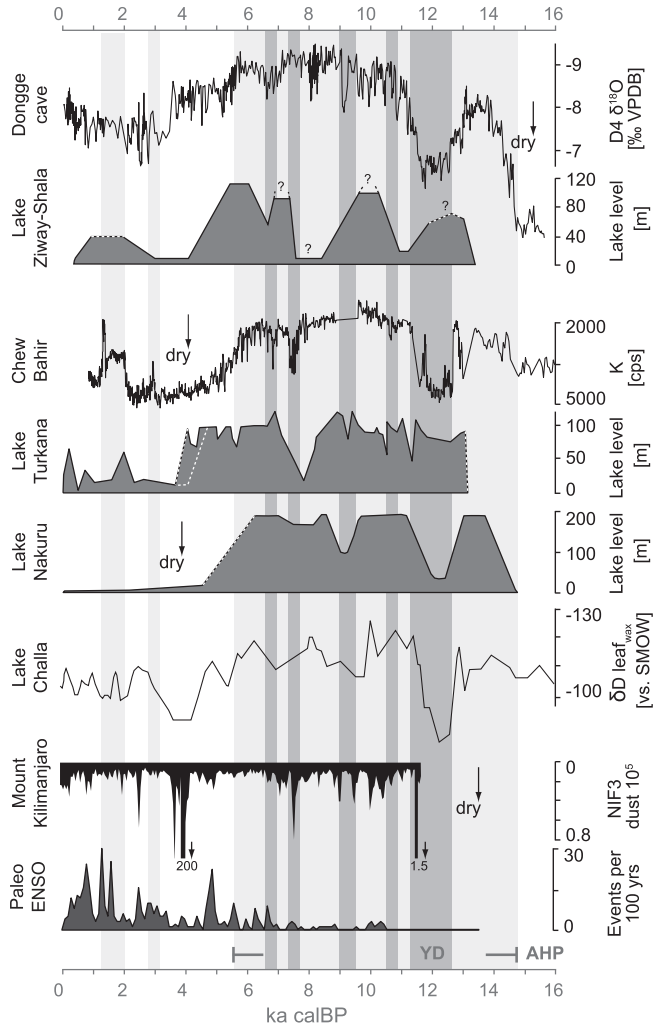

Fig. 6. Comparison of onset and termination of East African lake levels from Chew Bahir potassium (K) record (note reverse scale), lake Nakuru (Richardson and Dussinger, 1986), lake Ziway-Shala (Gillespie et al., 1983), and Lake Turkana (Johnson et al., 1991; Brown and Fuller, 2008) with the eolian dust record to Mt. Kilimanjaro (Thompson et al., 2002) due to enhanced aridity, hydrological proxy data from Lake Challa from δD leaf wax (Tierney et al., 2011), the oxygen-isotope records from Dongge cave (Dykoski et al., 2005), and the paleo-ENSO record from Laguna Pallcacocha, southern Ecuador (Moy et al., 2002). AHP – African Humid Period; YD – Younger Dryas; dark gray bars indicate dry episodes; light gray bars indicative for humid episodes.

(deMenocal et al., 2000; Morrill et al., 2003). An equally large body of evidence points to a gradual trend Towards aridity since ~7.8 ka (Fleitmann et al., 2003; Gupta et al., 2005; Wang et al., 2005; Asrat et al., 2007; Baker et al., 2010; Junginger, 2011). A highly nonlinear response of paleoclimate records implies that the abruptness of the termination of the AHP has been amplified considerably by feedback mechanisms as suggested by Claussen et al. (1999). deMenocal et al. (2000) differentiate between two feedback mechanisms that could have amplified such a transition: coupled vegetation-albedo feedback and ocean surface temperature-moisture feedback. Comparisons of lake level records located in the vicinity of Chew Bahir show large differences in the timing and abruptness of the AHP termination (Fig. 6). These differences are almost certainly due to local hydrological factors related to the topography of the lake basins and their catchments.

Following the termination of the AHP at 5 ka, arid conditions re-established and remained relatively stable until 2 ka, with one short abrupt excursion Towards more humid conditions around 3 ka. A longer humid interval began abruptly in two steps around 2 ka, and remained humid until 1.5 ka before terminating abruptly at 1.3 ka. The combined increase of Fe and Ti in the record hints at constant fluvial input as the dominant input system for that time. Dry conditions on a millennial scale are a common feature of tropical African paleo-climate archives such as that around 4 ka at Ziway-Shala (Gillespie et al., 1983) or Lake Turkana (Johnson et al., 1991; Fig. 6). The presence of a millennial-scale drought in the stalagmite records of southeast Asia (Wang et al., 2001) as well as marked aridity in Ethiopian speleothem records for these periods (Asrat et al., 2007; Baker et al., 2010), underlines the regional expression of this dry event. Possible mechanisms for such humidity shifts, out of phase with precessional forcing, may be related to an enhanced higher-frequency ENSO (El Niño/Southern Oscillation) causing more stable humid conditions (Fig. 6). Such enhanced periodicities in ENSO anomalies were observed for the 3–2.5 ka, 1.6 ka and 1.3 ka (Moy et al., 2002).

6. Conclusion

The sediment record from the Chew Bahir basin contains a number of valuable climate proxies that provide high resolution climate reconstructions for the past 45 ka, showing a distinct pattern of changing environmental conditions during the Late Quaternary in southern Ethiopia. These climate changes can be correlated to well-known wet–dry cycles for tropical east Africa (e.g., LGM, AHP, YD), and hint to a valuable age model even if it is based only upon six data points to date.

The Chew Bahir basin has been proven to be a suitable climate archive with well datable deposits without age reversals that give valuable insight into a highly variable environment. The sediment record comprises a number of meaningful proxies, foremost K, which enabled high resolution reconstructions of the climate variability in the region since 45 ka, based on the analysis of geochemical, physical and biological indicators. Sediment types have been analyzed and indicate that input mechanisms and provenances do vary and are clearly controlled by climate changes and can therefore help to understand regional shifts in moisture availability. With six to seven fold increased sedimentation rates during humid phases, Chew Bahir reacts very sensitively Towards even moderate climate changes and clearly reflects short-term variations on millennial timescales, like the latest one known as the Younger Dryas. Precession-forced long-term variations, such as the AHP, are expressed in the Chew Bahir basin, and appear to be synchronous with changes in Lake Malawi, Lake Tanganyika, West African marine cores, and the Hulu/Dongge Caves. This wet phase in Chew Bahir is marked by a stepwise, rather abrupt onset and a gradual termination.

Longer core records, to ~150 m depth, from the basin thus will offer the possibility of reconstructing the paleoenvironmental history since the origin of *H. sapiens* 200,000 years ago. Consequently, the site has great potential to shed light on the setting of evolution and dispersal of AMH, although only 45 ka at present. Further detailed analysis of a transect of cores through the basin will provide a better understanding of localized sedimentation in the lake and the mechanisms and processes behind the climate variations derived from these findings can be made evident from the sedimentary archive. It should also be possible to correlate the Chew Bahir results with archeological findings in the region (Brandt et al., 2012), testing models of the causes of population change and technological innovation in early human societies.

Acknowledgments

We are grateful to Addis Ababa University for support in making the field campaigns possible, and to Addis Geosystems Ltd for providing drilling equipment. Nina Bösche (University of Potsdam) assisted with satellite image processing, and Frederik von Reumont and Andreas Bolten helped with cartography. We would like to thank Martin Wessels and two anonymous reviewers whose comments greatly improved the manuscript. This project is affiliated to the CRC 806, which financially supported the first field campaign. The Chew Bahir Project is a contribution to the International Continental Scientific Drilling Program (ICDP), part of the ICDP-HSPDP initiative organized by A. Cohen. We thank the German Science Foundation (DFG) for funding all these projects.

References

Altabet, M.A., Higginson, M.J., Murray, D.W., 2002. The effect of millennial-scale changes in Arabian Sea denitrification on atmospheric CO_2. Nature 415, 159–162.

Ambrose, S.H., 1998. Late Pleistocene human population bottlenecks, volcanic winter, and the differentiation of modern humans. Journal of Human Evolution 35, 115–118.

Armitage, S.J., Jasim, S.A., Marks, A.E., Parker, A.G., Usik, V.I., Uerpmann, H.-P., 2011. Evidence for an early expansion of modern humans into Arabia. Science 331, 453–457.

Asrat, A., Baker, A., Umer, M., Moss, J., Leng, M., Van Calsteren, P., Smith, C., 2007. A high-resolution multi-proxy stalagmite record from Mechara, southeastern Ethiopia: palaeohydrological implications for speleothem palaeoclimate reconstruction. Journal of Quaternary Science 22, 53–63.

Asrat, A., Bates, R., Berger, G., Beyene, Y., Brandt, S., DeGusta, D., Duller, G., Ebinger, C., Endale, T., Hart, W.K., Hildebrand, E., Katoh, S., Kidane, T., Lamb, H., Leng, M., Lezine, A.-M., Marshall, M., Morgan, L., Pearce, N., Prave, T., Renne, P., Schäbitz, F., Strecker, M., Suwa, G., Tadesse, K., Tadesse, T., Trauth, M., Umer, M., Vogelsang, R., White, T., WoldeGabriel, G., Zeleke, A., 2009. The Chew Bahir Drilling Project: A Plio-Pleistocene Climate Record from the Southern Ethiopian Rift, a Crucible of Human Evolution. Proposal for the ICDP-HSPDP (Hominin Sites and Palaeolakes Drilling Project), pp. 1–8.

Baker, A., Asrat, A., Leng, M., Thomas, L., Fairchild, I.J., Widmann, M., Dong, B., Van Calsteren, P., Bryant, C., 2010. Decadal-scale rainfall variability in Ethiopia recorded in an annually laminated, Holocene-age, stalagmite. The Holocene 20, 827–836.

Barker, P.A., Talbot, M.R., Street-Perrott, F.A., Marret, F., Scourse, J., Odada, E.O., 2004. Late Quaternary variability in intertropical Africa. In: Battarbee, R.W., Gasse, F., Stickley, C.E. (Eds.), Past Climate Variability through Europe and Africa. Springer, Dordrecht, pp. 117–138.

Behrensmeyer, A.K., 2006. Climate change and human evolution. Science 311, 476–478.

Berger, A., Loutre, M.-F., 1991. Insolation values for the climate of the last 10 million years. Quaternary Science Reviews 10, 297–317.

Brandt, S.A., Fisher, E.C., Hildebrand, E.A., Vogelsang, R., Ambrose, S.H., Lesur, J., Wang, H., 2012. Early MIS 3 occupation of Mochena Borago Rockshelter, Southwest Ethiopian Highlands: implications for Late Pleistocene archaeology, paleoenvironments and modern human dispersal. Quaternary International 274, 38–54.

Bronk Ramsey, 2010. OxCal v4.1.7 Calibration Software. http://c14.arch.ox.ac.uk/embed.php%3fFile%3dindex.html (accessed 05.05.11.).

Brown, E.T., Fuller, C.H., 2008. Stratigraphy and tephra of the Kibish formation, southwestern Ethiopia. Journal of Human Evolution 55, 366–403.

Brown, E.T., Johnson, T., Scholz, C., Cohen, A., King, J., 2007. Abrupt change in tropical African climate linked to the bipolar seesaw over the past 55,000 years. Geophysical Research Letters 34 (L20702), 1–5.

Camberlin, P., 1997. Rainfall anomalies in the source region of the Nile and their connection with the Indian summer monsoon. Journal of Climate 10, 1380–1392.

Camberlin, P., Philippon, N., 2002. The east African March–May rainy season: associated atmospheric dynamics and predictability over the 1968–97 period. Journal of Climate 15, 1002–1019.

Carto, S.L., Weaver, A.J., Hetherington, R., Lam, Y., Wiebe, E.C., 2009. Out of Africa and into an ice age: on the role of global climate change in the late Pleistocene migration of early modern humans out of Africa. Journal of Human Evolution 56, 139–151.

Castañeda, I.S., Mulitza, S., Schefuss, E., Lopes de Santos, R.A., Damsté, J.S.S., Schouten, S., 2009. Wet phases in the Sahara/Sahel region and human migration patterns in North Africa. PNAS (Proceedings of the National Academy of Sciences) 106, 20159–22016.

Chalié, F., Gasse, F., 2002. Late Glacial-Holocene diatom record of water chemistry and lake level change from the tropical East African Rift Lake Abiyata (Ethiopia). Palaeogeography, Palaeoclimatology, Palaeoecology 187, 259–283.

Chase, B., Quick, L., Meadows, M., Scott, L., Thomas, D., Reimer, P., 2011. Late glacial interhemispheric climate dynamics revealed in South African hyrax middens. Geology 39, 19–22.

Clark, J., Beyene, Y., WoldeGabriel, G., Hart, W.K., Renne, P., Gilbert, E., Defleur, A., Suwa, G., Katoh, S., Ludwig, K.R., Boisserie, J.-R., Asfaw, B., White, T.D., 2003. Stratigraphic, chronological and behavioural contexts of Pleistocene *Homo sapiens* from Middle Awash, Ethiopia. Nature 423, 747–752.

Clark, P.U., Dyke, A.S., Shakun, J.D., Carlson, A.E., Clark, J., Wohlfarth, B., Mitrovica, J.X., Hostetler, S.W., McCabe, A.M., 2009. The Last Glacial Maximum. Science 325, 710–714.

Claussen, M., Kubatzki, C., Brovkin, V., Ganopolski, A., Hoelzmann, P., Pachur, H.J., 1999. Simulation of an abrupt change in Saharan vegetation in the mid-Holocene. Geophysical Research Letters 26, 2037–2040.

Clement, A.C., Seager, R., Cane, M.A., 1999. Orbital controls on the El Nino/Southern Oscillation and the tropical climate. Paleoceanography 14, 441–456.

Corti, G., 2009. Continental rift evolution: from rift initiation to incipient break-up in the Main Ethiopian Rift, East Africa. Earth-Science Reviews 96, 1–53.

Davidson, A., 1983. The Omo River project: reconnaissance geology and geochemistry of parts of Ilubabor, Kefa, Gemu Gofa and Sidamo. Ethiopian Institute of Geological Surveys Bulletin 2, 1–89.

deMenocal, P., Ortiz, J., Guilderson, T., Adkins, J., Sarnthein, M., Baker, L., Yarusinsky, M., 2000. Abrupt onset and termination of the African Humid Period: rapid climate responses to gradual insolation forcing. Quaternary Science Reviews 19, 347–361.

Diro, G.T., Grimes, D.I.F., Black, E., 2010. Teleconnections between Ethiopian summer rainfall and sea surface temperature; part I: observation and modeling. Climate Dynamics. http://dx.doi.org/10.1007/s00382-010-0837-8.

Dykoski, C.A., Edwards, R.L., Cheng, H., Yuan, D., Cai, Y., Zhang, M., Lin, Y., Qing, J., An, Z., Revenaugh, J., 2005. A high-resolution, absolute dated Holocene and deglacial Asian monsoon record from Dongge Cave, China. Earth and Planetary Science Letters 233, 71–86.

Ebinger, C.J., Yemane, T., Harding, D., Tesfaye, S., Kelley, S., Rex, D., 2000. Rift deflection, migration, and propagation: linkage of the Ethiopian and Eastern rifts, Africa. Geological Society of America Bulletin 112, 163–176.

Fleitmann, D., Burns, S.J., Mudelsee, M., Neff, U., Kramers, J., Mangini, A., Matter, A., 2003. Holocene forcing of the Indian monsoon recorded in a stalagmite from Southern Oman. Science 300, 1737–1739.

Garcin, Y., Junginger, A., Melnick, D., Olago, D., Strecker, M., Trauth, M.H., 2009. Late Pleistocene–Holocene rise and collapse of the Lake Suguta, northern Kenya Rift. Quaternary Science Reviews 28, 911–925.

Gasse, F., 1986. East African Diatoms – Taxonomy, Ecological Distribution. J. Cramer in der Gebrüder Borntager Verlagsbuchhandlung, Berlin, Stuttgart.

Gasse, F., 2000. Hydrological changes in the African tropics since the Last Glacial Maximum. Quaternary Science Reviews 19, 189–211.

Gasse, F., Van Campo, E., 1994. Abrupt post-glacial climate events in West Asia and North Africa monsoon domains. Earth and Planetary Science Letters 126, 435–456.

Gasse, F., Street, F.A., 1978. Late Quaternary lake level fluctuations and environments of the northern Rift Valley and Afar Region (Ethiopia and Djibouti). Palaeogeography, Palaeoclimatology, Palaeoecology 25, 145–150.

Gasse, F., Chalié, F., Vincens, A., Williams, M.A.J., Williamson, D., 2008. Climatic patterns in equatorial and southern Africa from 30,000 to 10,000 years ago reconstructed from terrestrial and near-shore proxy data. Quaternary Science Reviews 27, 2316–2340.

Gillespie, R., Street-Perrott, F.A., Switsur, R., 1983. Post-glacial arid episodes in Ethiopia have implications for climate prediction. Nature 306, 680–683.

Guo, Z., Petit-Maire, N., Kröpelin, S., 2000. Holocene non-orbital climatic events in present-day arid areas of northern Africa and China. Global and Planetary Change 26, 97–103.

Gupta, A.K., Das, M., Anderson, D.M., 2005. Solar influence on the Indian summer monsoon during the Holocene. Geophysical Research Letters 32, L17703. http://dx.doi.org/10.1029/2005GL022685.

Hailemichael, M., Aronson, J.L., Savin, S., Tevesz, M.J.S., Carter, J.G., 2002. $\delta^{18}O$ in mollusk shells from Pliocene Lake Hadar and modern Ethiopian lakes: implications for history of the Ethiopian monsoon. Palaeogeography, Palaeoclimatology, Palaeoecology 186, 81–99.

Hildebrand, E.A., Brandt, S.A., Lesur-Gebremariam, J., 2010. The Holocene archaeology of southwest Ethiopia: new insights from the Kafa Archaeological project. African Archaeological Review 27 (2), 55–289.

Johnson, T.C., Halfman, J.D., Showers, W.J., 1991. Paleoclimate of the past 4000 years at Lake Turkana, Kenya, based on the isotopic composition of authigenic calcite. Palaeogeography, Palaeoclimatology, Palaeoecology 85, 189–198.

Joordens, J.C.A., Vonhof, H.B., Feibel, C.S., Lourens, L.J., Dupont-Nivet, G., Van der Lubbe, H.J.L., Sier, M., Davies, G.R., Kroon, D., 2011. An astronomically-tuned climate framework for hominins in the Turkana Basin. Earth and Planetary Science Letters 307, 1–8.

Junginger, A., 2011. East African Climate Variability on Different Time Scales: The Suguta Valley in the African–Asian Monsoon Domain. Ph.D. thesis, University of Potsdam, Germany. http://opus.kobv.de/ubp/volltexte/2011/5683/

Kröpelin, S., Verschuren, D., Lézine, A.-M., Eggermont, H., Cocquyt, C., Francus, P., Cazet, J.-P., Fagot, M., Rumes, B., Russell, J.M., Darius, F., Conley, D.J., Schuster, M., von Suchodoletz, H., Engstrom, D.R., 2008. Climate-driven ecosystem succession in the Sahara: the past 6000 years. Science 320, 765–768.

Kutzbach, J.E., Street-Perrott, F.A., 1985. Milankovitch forcing of fluctuations in the level of tropical lakes from 18 to 0 kyr BP. Nature Geoscience 317, 130–134.

Leng, M.J., Lamb, A.L., Lamb, H.F., Telford, R.J., 1999. Palaeoclimatic implications of isotopic data from modern and early Holocene shells of the freshwater snail *Melanoides tuberculata*, from lakes in the Ethiopian Rift Valley. Journal of Paleolimnology 21, 97–106.

Martínez, I., Keigwin, L., Barrows, T.T., Yokoyama, Y., Southon, J., 2003. La Niña-like conditions in the eastern equatorial Pacific and a stronger Choco jet in the northern Andes during the last glaciation. Paleoceanography 18, 1033.

McDougall, I., Brown, F.H., Fleagle, J.G., 2005. Stratigraphic placement and age of modern humans from Kibish, Ethiopia. Nature 433, 733–736.

Meyers, P.A., 2003. Applications of organic geochemistry to paleolimnological reconstructions: a summary of examples from the Laurentian Great Lakes. Organic Geochemistry 34, 261–289.

Moore, J.M., Davidson, A., 1978. Rift structure in southern Ethiopia. Tectonophysics 46, 159–173.

Morrill, C., Overpeck, J.T., Cole, J.E., 2003. A synthesis of abrupt changes in the Asian summer monsoon since the last deglaciation. Holocene 13, 465–476.

Moy, C.M., Seltzer, G.O., Rodbell, D.T., Anderson, D.M., 2002. Variability of El Niño/Southern Oscillation activity at millennial timescales during the Holocene epoch. Nature 420, 162–165.

Nicholson, S.E., 1996. A review of climate dynamics and climate variability in eastern Africa. In: Johnson, T.C., Odada, E.O. (Eds.), The Limnology, Climatology and Paleoclimatology of the East African Lakes. Gordon & Breach, Amsterdam, pp. 25–56.

North Greenland Ice Core Project members, 2004. High-resolution record of northern hemisphere climate extending into the last interglacial period. Nature 431, 147–151.

Okoola, R., 1999. A diagnostic study of the Eastern African monsoon circulation during the northern hemisphere spring season. International Journal of Climatology 19, 143–168.

Olaka, L.A., Odada, E.O., Trauth, M.H., Olago, D.O., 2010. The sensitivity of East African rift lakes to climate fluctuations. Journal of Paleolimnology 44, 629–644.

Oppenheimer, S., 2009. The great arc of dispersal of modern humans: Africa to Australia. Quaternary International 202, 2–13.

Partridge, T.C., Lowe, J., Barker, P., Hoelzmann, P., Magri, D., Saarnisto, M., Vandenberghe, J., Street-Perrott, F., Gasse, F., 2004. Climate Variability in Europe and Africa: a PAGES-PEP III Time Stream II Synthesis. Springer, Dordrecht.

Pik, R., Marty, B., Carignan, J., Yirgu, G., Ayalew, T., 2008. Timing of East African Rift development in southern Ethiopia: Implication for mantle plume activity and evolution of topography. Geology 36, 167–170.

Pointier, J.P., Delay, B., Toffart, J.L., Lefevre, M., Romero-Alvarez, R., 1992. Life history traits of three morphs of *Melanoides tuberculata* (Gastropoda: Thiaridae), an invading snail in the French West Indies. Journal of Molluscan Studies 58, 415–423.

Potts, R., 1998. Environmental hypotheses of hominin evolution. Yearbook of Physical Anthropology 41, 93–136.

Reimer, P.J., Baillie, M.G.L., Bard, E., Bayliss, A., Beck, J.W., Blackwell, P.G., Bronk Ramsey, C., Buck, C.E., Burr, G.S., Edwards, R.L., Friedrich, M., Grootes, P.M., Guilderson, T.P., Hajdas, I., Heaton, T.J., Hogg, A.G., Hughen, K.A., Kaiser, K.F., Kromer, B., McCormac, F.G., Manning, S.W., Reimer, R.W., Richards, D.A., Southon, J.R., Talamo, S., Turney, C.S.M., van der Plicht, J., Weyhenmeyer, C.E., 2009. INTCAL09 and MARINE09 radiocarbon age calibration curves, 0–50,000 years cal BP. Radiocarbon 51, 1111–1150.

Renssen, H., Brovkin, V., Fichefet, T., Goosse, H., 2006. Simulation of the Holocene climate evolution in northern Africa: the termination of the African humid period. Quaternary International 150, 95–102.

Rethemeyer, J., Fülöp, R., Höfle, S., Wacker, L., Heinze, S., Hajdas, I., Patt, U., König, S., Stapper, B., Dewald, A. Status report on sample preparation facilities for ^{14}C analysis at the new CologneAMS center. Nuclear Instruments and Methods in Physics Research B, in press.

Richardson, J.L., Dussinger, R.A., 1986. Paleolimnology of mid-elevation lakes in the Kenya Rift Valley. Hydrobiologia 143, 167–174.

Richardson, J.L., Richardson, A.E., 1972. History of an African Rift lake and its climatic implications. Ecological Monographs 42, 499–534.

Segele, Z.T., Lamb, P.J., 2005. Characterization and variability of Kiremt rainy season over Ethiopia. Meteorology and Atmospheric Physics 89, 153–180.

Shanahan, T.M., Overpeck, J.T., Wheeler, C.W., Beck, J.W., Pigati, J.S., Talbot, M.R., Scholz, C.A., Peck, J., King, J.W., 2006. Paleoclimatic variations in West Africa from a record of late Pleistocene and Holocene Lake level stands of Lake Bosumtwi, Ghana. Palaeogeography, Palaeoclimatology, Palaeoecology 242, 287–302.

Stabel, H.H., 1987. Coupling of strontium and calcium cycles in Lake Constance. Hydrobiologia 176–177, 323–329.

Stager, J., Ryves, D., Chase, B., Pausata, F., 2011. Catastrophic drought in the Afro-Asian monsoon region during Heinrich Event 1. Science 331, 1299–1302.

Stringer, C., 2003. Out of Ethiopia. Nature 423, 692–695.

Telford, R.J., Lamb, H.F., 1999. Groundwater-mediated response to Holocene climatic change recorded by the diatom stratigraphy of an Ethiopian crater lake. Quaternary Research 52, 63–75.

Thompson, L.G., Mosley-Thompson, E., Davis, M.E., Henderson, K.A., Brecher, H.H., Zagorodnov, V.S., Mashiotta, T.A., Lin, P.-N., Mikhalenko, V.N., Hardy, D.R., Beer, J., 2002. Kilimanjaro ice core records: evidence of Holocene climate change in Tropical Africa. Science 298, 589–593.

Tierney, J.E., Russell, J.M., Huang, Y., Sinninghe Damsté, J.S., Hopmans, E.C., Cohen, A., 2008. Northern hemisphere controls on tropical Southeast African climate during the past 60,000 years. Science 322, 252–255.

Tierney, J.E., Russell, J.M., Sinninghe Damsté, J.S., Huang, Y., Verschuren, D., 2011. Late Quaternary behavior of the East African monsoon and the importance of the Congo Air Boundary. Quaternary Science Reviews 30, 798–807.

Trauth, M.H., Deino, A.L., Bergner, A.G.N., Strecker, M.R., 2003. East African climate change and orbital forcing during the last 175 kyr BP. Earth and Planetary Science Letters 206, 297–313.

Trauth, M.H., Maslin, M.A., Deino, A.L., Junginger, A., Lesoloyia, M., Odada, E.O., Olago, D.O., Olaka, L.A., Strecker, M.R., Tiedemann, R., 2010. Human evolution in a variable environment: the amplifier lakes of Eastern Africa. Quaternary Science Reviews 29, 2981–2988.

Vrba, E.S., 1985. Environment and evolution: alternative causes of the temporal distribution of evolutionary events. South African Journal of Sciences 81, 229–236.

Wacker, L., Fülöp, R., Hajdas, I., Molnár, M., Rethemeyer J. A novel approach to process carbonate samples for radiocarbon measurement. Nuclear Instruments and Methods in Physics Research B, submitted for publication.

Wang, Y.J., Cheng, H., Edwards, R.L., An, Z.S., Wu, J.Y., Shen, C.-C., Dorale, J.A., 2001. A high-resolution absolute-dated late Pleistocene monsoon record from Hulu Cave, China. Science 294, 2345–2348.

Wang, Y.J., Cheng, H., Edwards, R.L., He, Y., Kong, X., An, Z., Wu, J., Kelly, M.J., Dykoski, C.A., Li, X., 2005. The Holocene Asian monsoon: links to solar changes and North Atlantic climate. Science 308, 854–857.

White, T.D., Asfaw, B., DeGusta, D., Gilbert, H., Richards, G.D., Suwa, G., Howell, F.C., 2003. Pleistocene *Homo sapiens* from Middle Awash, Ethiopia. Nature 423, 742–747.

Williams, A.P., Funk, C., 2011. A westward extension of the warm pool leads to a westward extension of the Walker circulation, drying eastern Africa. Climate Dynamics. http://dx.doi.org/10.1007/s00382-010-0984-y.

Yuan, D., Cheng, H., Edwards, R.L., Dykoski, C.A., Kelly, M.J., Zhang, M., Qing, J., Lin, Y., Wang, Y., Wu, J., Dorale, J.A., An, Z., Cai, Y., 2004. Timing, duration, and transitions of the Last Interglacial Asian Monsoon. Science 304, 575–578.